
Preliminary Aerodynamic Design of a Fan Stage for an Ultra High Bypass Ratio Engine

Daniel Giesecke, Jens Friedrichs
d.giesecke@ifas.tu-braunschweig.de

Technische Universität Braunschweig
Institute of Jet Propulsion and Turbomachinery
Braunschweig
Germany

Udo Stark

Technische Universität Braunschweig
Institute of Fluid Mechanics
Braunschweig
Germany

ABSTRACT

In the framework of the Coordinated Research Centre 880 (Sonderforschungsbereich 880) the fundamentals of an environmental friendly future regional aircraft are being developed. Therefore, an engine with a bypass ratio of 17 for the target reference aircraft mission has to be designed resulting in an increased propulsive efficiency. In order to reduce the adverse viscous drag effects of a large intake for such ultra high bypass ratio engines, the intake will be reduced in its length. With this background, the engine installation position was chosen above the wing to realize some noise shielding effects as well as inflow straightening effects. To investigate the inflow situation and interaction a suitable transonic fan stage has to be developed.

The paper describes the design process starting from aircraft specifications to an engine performance model and a preliminary fan stage design. The preliminary fan stage design procedure relies on the isentropic simple-radial equilibrium equation. The blade sections are parabolic mean lines with cubic thickness distributions. During the design process special attention has been drawn on the supersonic flow approaching the rotor leading edge resulting in a complex shock structure. The shock structure goes hand-in-hand with the incidence chosen. Firstly, a peak isentropic efficiency of 87 percent was achieved with a large in- and outlet duct. Secondly, numerical simulations using isolated nacelle flow by cutting away the inlet duct show an increase in isentropic efficiency to almost 88 percent at design point.

To summarize, numerical verifications show consistent results with the design specification and hence, methodology used. Further inflow investigations in case of the on-wing mounted engine will be part of the on-going research project.

NOMENCLATURE

Symbols

| | |
|-----------------|---|
| a, b | camber line parameter |
| $a - f$ | thickness coefficients |
| c | chord length |
| D | diffusion factor |
| f | maximum camber |
| H | blade height |
| m | deviation parameter |
| \dot{m}_{red} | reduced mass flow |
| N_{fan} | fan rotational speed |
| p_t | total pressure |
| r | radius |
| R | tip radius |
| s | spacing |
| t_1 | leading edge thickness |
| t_2 | trailing edge thickness |
| T | maximum thickness |
| V | velocity |
| X | x coordinate of the camber line (dimensionless) |
| X_T | position of maximum thickness (dimensionless) |
| X_f | position of maximum camber (dimensionless) |
| Y_c | y coordinate of the camber line (dimensionless) |
| Y_{t1} | thickness upstream of X_T (dimensionless) |
| Y_{t2} | thickness downstream of X_T (dimensionless) |
| β'_1 | relative velocity angle at rotor inlet |
| β'_2 | relative velocity angle at rotor outlet |
| δ | deviation |
| ϕ | camber angle |
| η_{is} | isentropic efficiency |
| ΔSFC | SFC change |
| ΔSM | surge margin change |

Subscripts

| | |
|-----------------|-------------------------------------|
| 1 | rotor inlet station |
| i | i th streamline |
| Ro | Rotor |
| <i>safety</i> | distance to 15 percent surge margin |
| <i>standard</i> | standard fan map |
| St | Stator |
| $UHBR$ | UHBR fan map |
| z | axial |
| θ | circumferential |

Abbreviations

| | |
|--------------|--|
| ACARE | Advisory Council of Aeronautics Research in Europe |
| AEO | all engine operating |
| BPR | bypass ratio |
| CRC | Coordinated Research Centre |
| CS | Certification Specification |
| DLR | German Aerospace Centre |
| EASA | European Aviation Safety Agency |
| FPR | fan pressure ratio |
| IATA | International Air Transport Association |
| ISRE | isentropic simple radial equilibrium |
| LNF | low noise fan |
| MIT | Massachusetts Institute of Technology |
| NASA | National Aeronautics and Space Administration |
| OEI | one engine inoperative |
| OPR | overall pressure ratio |
| <i>PrADO</i> | Preliminary Aircraft Design and Optimization |
| RANS | Reynolds-averaged Navier-Stokes |
| SFC | specific fuel consumption |
| TET | turbine entry temperature |
| TOC | top of climb |
| TU | Technische Universität |
| UHBR | ultra-high bypass ratio |

1.0 INTRODUCTION

Recent studies from the International Air Transport Association (IATA) [1] show a double of passengers in 2035. The largest percentage growth will be in Africa (5.1 percent) followed by the Middle East (4.8 percent), Asia Pacific (4.7 percent) and Latin America (3.8 percent). But also the North American and Europe will further increase in growth by 2.8 percent and 2.5 percent. The Advisory Council of Aeronautics Research in Europe (ACARE) announced in 2001 the "Vision for 2020" [2] in order to define how aviation technologies have to develop to reduce the environmental footprint. Those guidelines were adapted in 2011 by the ACARE within the "Flightpath 2050" [3]. The main targets are the reduction of perceived noise emission by 65 percent, CO_2 and NO_x emission reduction by 75 and 90 percent. Obviously, a further reduction of fuel consumption is required too. Remaining the high safety standards, several operational targets were added to the guidelines such as faster point-to-point connections to ensure 90 percent of travelers finish their door-to-door journey in Europe within 4 hours. This requires a larger usage of regional airports which are located all over Europe and would reduce the capacity problems main hub airports already have nowadays.

Regarding the fuel consumption reduction, Daggett et al. [4] showed that both, changing the engine cycle and increasing the bypass ratio (BPR) from 14.3 to 21.5 have a beneficial effect on specific fuel consumption (SFC) of about 14 percent. In that case, the operating costs of a re-sized conventional aircraft drops by 16 percent. One engine cycle investigated in the study [4] was similar to the geared P&W1100G turbofan engine which got into service recently. The P&W engine features a BPR of 12.5 with a gearbox between the fan rotor and

the low speed shaft. The BPR of the geared turbofan engine investigated in Daggett et al. [4] was even further increased from 14.3 to 21.5. This resulted in an overall pressure ratio (OPR) of up to 70 and a fan pressure ratio (FPR) below 1.45. One challenge of engines with such large BPR and hence, large engine diameter is the engine-wing mount. Conventional aircraft designs with larger BPR engines already show the typical interaction effects when the engine moves further to the aircraft wing leading edge due to the legally defined nacelle to ground distance.

Usually, ultra-high bypass ratio (UHBR) designs are characterized by a larger propulsive efficiency which is due to larger BPR, hence, engine mass flow and lower exit velocity at the bypass nozzle. This again is a result of the low specific thrust cycle because of the lower FPR. A lower bypass nozzle velocity incorporates less boundary layer interaction noise between nozzle and flight velocity leading to kind of a shielding effect.

To address the future challenges not only the engine but also the aircraft design have to be adjusted. Therefore, within the Coordinated Research Centre 880 (CRC 880) the fundamentals of an active high-lift single-aisle aircraft are investigated. The aircraft features an UHBR engine to benefit from the lower fuel consumption. Further to that, the engines are mounted over the wing which add a further shielding of the fan noise. The aircraft is supposed to take off and land on runway with a maximum length of 900 *m*. This would allow the usage of regional airports in order to achieve faster point-to-point connections within Europe. However, one drawback of this engine installation is the particular inflow compared to conventional aircraft designs with the nacelle in front and above the wing. Therefore, the interaction of inflow and fan needs to be investigated in further detail which requires a preliminary fan stage design for UHBR engines.

In open literature only a very few transonic fan stage designs are described. Several rotor stage designs of a high mach number blading are reported by Gostelow et al. [5]. The rotor only stages were designed for a corrected mass flow of 97.7 *kg/sec* and a pressure ratio of 1.6. The tip diameter was 0.927 *m* with a hup to tip ratio of 0.5. The experimental results show a rotor efficiency of 85.4 up to 89.5 percent depending on the tip airfoil geometry. Double circular arc airfoils without and with changed supersonic camber were designed. However, for all cases a 20 percent radial distortion show substantial reduction in mass flow (about 2.5 percent), surge margin (up to almost 20 percent) and peak efficiency (up to 7.8 percent). This emphasizes the inflow distortion effects on a fan stage.

Within a NASA research program Dalton et al. [6] describes low speed fan stage designs for lower noise emission. The stages differ in rotor-to-stator spacing and vane leading edge sweep. The fan stages with a hup to tip ratio of 0.3 featured a pressure ratio of 1.378 at a mass flow of 46 *kg/sec*. The rotor and stator blading is characterized by multiple respectively double circular arc airfoils. Rotor sections at transonic regions were tailored to match the shock structure at design point. Thereby, the maximum thickness of stator sections was positioned forward of mid chord. In the Cambridge-MIT Silent Aircraft Initiative [7] a preliminary fan design for a blended-wing body aircraft was determined by taking into account noise effects. The rotor design led to 20 blades and a design tip speed of 350 *m/sec* with a fan pressure ratio of 1.45. A rotor polytropic efficiency of 93.5 percent was achieved at top of climb condition. The lightly loaded rotor tip at take off resulted in low fan source noise. The fan rig of Kaplan [8] describes a low noise fan stage design for UHBR engines with a bypass ratio, pressure ratio and mass flow at top of climb (TOC) of 11.4, 1.44 and 102.6 *kg/sec* respectively. The rig test results show a peak isentropic efficiency of around 86 percent at take off rotational speed. The blading was generated with 31 variables for defining four splines.

The present paper aims at designing a preliminary fan stage design for further inlet distortion investigations in case of an UHBR engine which is mounted over the wing and partly embedded into the wing. Hence, the objective is a closed loop design starting with the aircraft description to the presentation of the UHBR engine and a final assessment of a preliminary fan stage design. This includes a simple examination of off-design operating points in the fan characteristics and in case of an isolated nacelle with clean inflow. Investigating the inflow distortion for the partly wing-embedded engine will be part of the on-going research program.

2.0 AIRCRAFT DESIGN

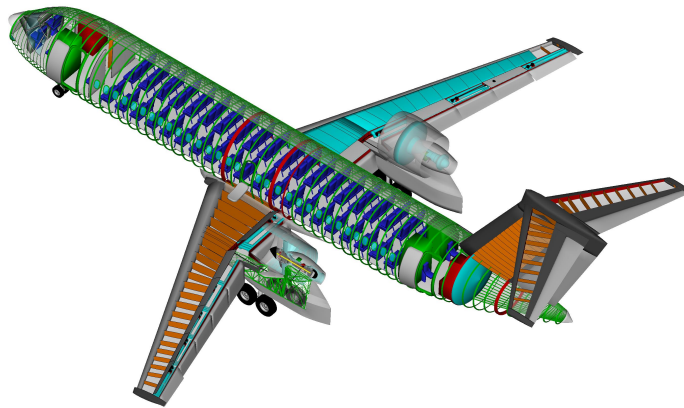


Figure 1. Engine over wing mounted aircraft configuration REF3-2015 within the CRC 880 [9].

All the technologies developed within the CRC 880 are reviewed in an assessment (e.g. direct operating costs, feasibility, etc.) within the Preliminary Aircraft Design and Optimization (*PrADO*) [10] tool which is an iterative overall aircraft design software and an in-house development by the Institute of Aircraft Design and Lightweight Structures (IFL) at TU Braunschweig over the last few decades. The specifications of the single-aisle aircraft are defined in accordance to the above-mentioned guidelines [2, 3] defined by the ACARE. Therefore, the aircraft has a maximum payload of 12000 kg for 100 passengers and freight. The flight mission is 2000 km with fuel for an alternative airport within 370 km and a holding flight of about 30 minutes. The flight Mach number is 0.78 at a cruising altitude of 11.277 km. The aircraft has to take off and land at runway lengths of maximum 900 m at sea level. The multidisciplinary approach between aircraft aerodynamics, flight mechanics and control, lightweight structures and jet engine data used in *PrADO*, results in a detailed aircraft geometry shown in Fig. 1. The assessment of the specific fuel consumption (SFC) and its noise emission of the propulsion system in context with the direct operating costs of the chosen aircraft configuration is part of study yet to be published.

Based on the iterative design process one design and several off design operating points

were estimated and are listed in Tab. 1. Besides usual operating points in which all engine are operating (AEO), several emergency cases with one engine inoperative (OEI) and EASA CS-25 certification cases exits and the engine has to cope with them too.

Table 1
Design and off design operating points

| Case | Operating Point | Height [m] | Mach [-] | Power Offtake [kW] | Bleed Air [kg/s] | Required Thrust [kN] |
|------|----------------------------|---------------|-------------|--------------------------|------------------------|----------------------------|
| 1 | Top of Climb, AEO | 11277 | 0.74 | 11.8 | 0.44 | 18.8 |
| 2 | Cruise, AEO | 11277 | 0.78 | 11.8 | 0.44 | 16.0 |
| 3 | Take-off, OEI ¹ | 11 | 0.17 | 764.9 | 0.88 | 71.7 |
| 4 | Lift-off point, OEI | 0 | 0.17 | 764.9 | 0.88 | 100.0 |
| 5 | Take-off, AEO | 0 | 0 | 382.5 | 0.44 | 129.9 |
| 6 | Take-off, OEI | 0 | 0 | 764.9 | 0.88 | 120.0 |
| 7 | Approach, OEI ¹ | 457 | 0.18 | 752.4 | 0.88 | 65.6 |
| 8 | Landing, AEO ¹ | 15 | 0.17 | 421.8 | 0.44 | 43.6 |
| 9 | Landing, OEI | 15 | 0.17 | 843.6 | 0.88 | 74.0 |
| 10 | Cruise, OEI | 5400 | 0.40 | 23.6 | 0.88 | 34.5 |
| 11 | Cruise, AEO | 12000 | 0.78 | 11.8 | 0.44 | 14.7 |

¹ = EASA CS-25.

3.0 ENGINE DESIGN

The *PrADO* tool has been extended by a data management system allowing a communication with the commercial engine cycle simulation tool *GasTurb* [11]. *GasTurb* provides several engine cycles and in particular characteristic curves for each engine module depending on ambient conditions, engine mass flow, bypass ratio (BPR), turbine entry temperature (TET) and component efficiencies. For the present study a technology readiness date of 2015 was selected following extrapolated trends [12]. It has to be highlighted that for the operating cases in Tab. 1 an implementation of the non-negligible bleed air and power offtake is vital.

Typically, the TOC condition is chosen for engine cycle designs. However, a safe operation for all other cases in Tab. 1 was ensured as well and are regarded as off design operating points. For the UHBR engine design a BPR of 17 with an OPR of 70 and a TET of 1750 K at TOC were determined. There, the fan has a pressure ratio of 1.42 which is comparable to other UHBR engine designs, e.g. Hall [13], at a reduced mass flow of 607.7 kg/sec. This led to a relatively low SFC (13.36 g/Ns). The gear ratio is 3.3 and also in accordance to recent geared turbofan designs.

4.0 PRELIMINARY FAN DESIGN

4.1 Meridional Plane

The starting point of any compressor design is the calculation of the meridional plane and hence, annulus area variation in order to estimate the distribution of flow conditions for ro-

tor and stator blade row. The present meridional plane design bases on the methodology explained by Giamati and Finger [14].

The first step is the determination of the basic flow equations of real compressible fluid such as the equation of state and the energy, continuity and the Navier-Stokes equations. Several assumptions are applied such as negligible blade forces, steady axial symmetric flow, no local shearing effects of viscosity and no heat transfer. In addition to the prescribed assumptions, the negligence of radial velocity entropy change along blade height, the so-called "simplified radial equilibrium" condition [14] is derived. For a circumferential averaged entropy which is radially constant, the "isentropic simple radial equilibrium" (ISRE) equation is obtained which has been used in the present preliminary design. The core element is the ISRE equation [14] and is expressed as:

$$V_z^2 - V_{z,i}^2 = 2c_p (T - T_i) - (V_\theta^2 - V_{\theta,i}^2) - \int_{r_i}^r \frac{2V_\theta^2}{r} dr \quad \dots (1)$$

Referring to Cumpsty [15], the effect of streamline curvature is considered to be relatively small for the chosen design.

Required input parameters are the rotor inlet flow conditions, rotor hub radius at inlet, rotor tip radius at outlet which corresponds to stator hub radius at its inlet, and stator tip radius at its outlet. These parameters were obtained by the *GasTurb* UHBR model. All the other geometry parameter were iteratively calculated to obtain the area change per streamline based on density change and the conservation of mass. This yields to a hub to tip ratio at rotor inlet of 0.35 which is accordance to the *GasTurb* UHBR model.

As reference designs the low speed fan stage for low noise emissions by Dalton [6] and the DLR UHBR fan stage by Kaplan [8] have been taken into account. The low noise fan (LNF) of NASA [6] the UHBR fan design from the DLR [8] had 18 rotor and 42 stator vanes respectively 22 rotor and 68 stator vanes. A rotor blade number of 19 was selected for the chosen fan design. The stator blade number was estimated by the well-known acoustic cut off condition [16] which results in a stator blade number of 55. As a result of the high flow turning at rotor hub, the stator is highly loaded which can be observed by the diffusion factor of almost 0.6, cf. Fig. 2 and 3. At design mass flow a FPR of 1.46 were obtained by the ISRE equation which is slightly higher than the *GasTurb* model with 1.42. This was achieved by a rotational speed of 3074 *rpm* and leads to an isentropic efficiency of 89.8 percent. At *GasTurb* an isentropic fan efficiency of 88.5 percent was assumed, again, based on the extrapolated trends in [12]. The low FPR of 1.46 results in a relative Mach number at rotor leading edge of almost 1.35. This is accordance to Crichton et al. [7] whose design had 1.45 as FPR and 1.28 as relative inflow Mach number. The LNF design of Dalton et al. [6] is characterized by a PR and relative Mach number of 1.378 and 1.143 respectively.

4.2 Airfoil Geometry Design

For each streamline the airfoil section was generated by superimposing the advanced parabolic mean arc line [17] and a cubic thickness distribution [18] applying the method from Abbott and von Doenhoff [19]. Hence, the mean arc line and the thickness distribution are generated separately, cf. Figures 4 and 5. Both fan rotor and stator, uses same blade airfoil generation technique which is different compared to the designs of Gostelow et al. [5] and Dalton et al. [6] with double respectively multiple circular arc airfoils.

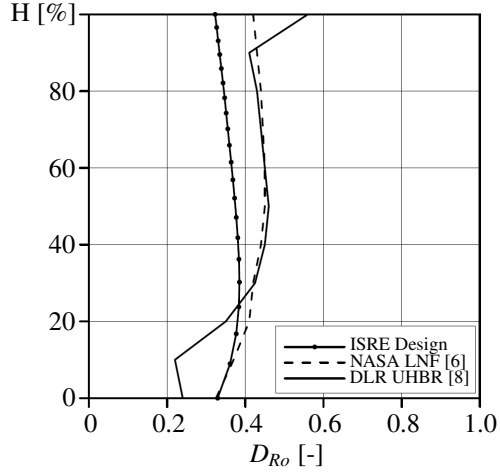


Figure 2. Rotor diffusion factor in comparison to NASA [6] and DLR [8] UHBR fan designs

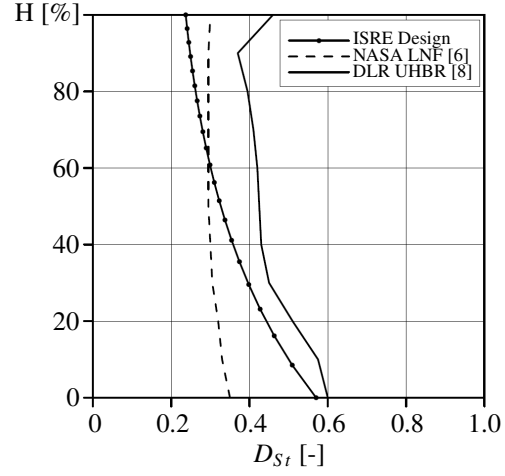


Figure 3. Stator diffusion factor in comparison to NASA [6] and DLR [8] UHBR fan designs

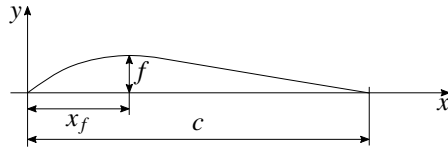


Figure 4. Parabolic mean arc line referring to Schlichting and Truckenbrodt [17]

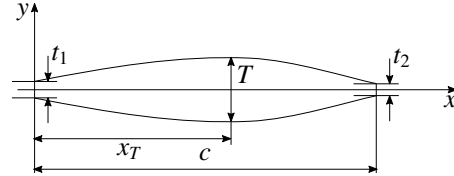


Figure 5. Cubic thickness Distribution referring to Wennerstrom [18]

The advantage of the advanced parabolic mean arc line is the absence of the inflection point as it is defined as one parabola lying somehow in the two-dimensional plane. Following Schlichting and Truckenbrodt [17], it is expressed in the dimensionless way as

$$Y_c(X) = a \cdot \frac{X(1-X)}{1+bX} \quad \dots (2)$$

with the parameters a and b which include the position of the maximum camber X_f , the chord length c and the maximum camber f :

$$a = \frac{f}{X_f^2 c}$$

and

$$b = \frac{1-2X_f}{X_f^2}$$

Besides, the flow turning a deviation was included for determine the camber angle ϕ which was adjusted by a scaling factor iteratively. The well-known empirical rule for deviation [14] is defined as:

$$\delta = m \cdot \phi \cdot \sqrt{\frac{s}{c}} \quad \dots (3)$$

where, referring to Saravanamuttoo [20],

$$m = 0.23 (2X_f)^2 + 0.1 \left(\frac{\beta'_2}{50} \right). \quad \dots(4)$$

In order to attain the required mass flow, attention during rotor design was paid to the "unique incidence" condition referring to Cumpsty [15]. At supersonic inflow velocity a particular stagger angle is needed to match inflow condition and airfoil geometry.

As already mentioned, the cubic thickness distribution according to Wennerstrom [18] was used. Depending whether the position of maximum thickness X_T is below or above 0.5, the thickness distribution is defined differently. However, for $X_T \geq 0.5$ the airfoil half-thickness upstream X_T is calculated as

$$Y_{t1}(X) = a \cdot X^3 + b \cdot X^2 + c \cdot X + d \quad \dots(5)$$

whereas, the thickness downstream X_T is

$$Y_{t2}(X) = e(X - X_T)^3 + f(X - X_T)^2 + g(X - X_T) + h. \quad \dots(6)$$

The coefficients a to d are estimated as follows

$$a = \frac{\left(\frac{t_1}{2} - \frac{T}{2} \right)}{(1 - X_T)^3}, \quad b = 0, \quad c = \frac{-3}{\left(2X_T \frac{t_1}{2} - \frac{T}{2} \right)}, \quad d = \frac{t_1}{2}$$

and e to h are

$$e = \frac{\left(\frac{t_2}{2} - \frac{T}{2} \right)}{(1 - X_T)^3} - \left(\frac{3}{2X_T^2} \right) + \frac{\frac{t_1}{2} - \frac{T}{2}}{1 - X_T}, \quad f = \left(\frac{3}{2X_T^2} \right) \cdot \left(\frac{t_1}{2} - \frac{T}{2} \right), \quad g = 0, \quad h = \frac{T}{2}.$$

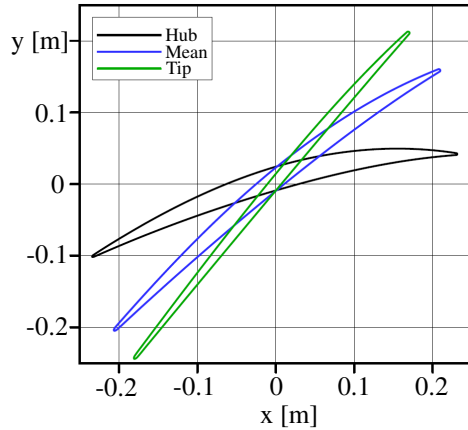


Figure 6. Rotor hub, mean and tip sections.

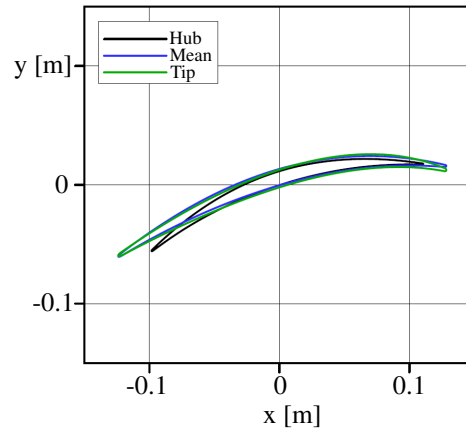


Figure 7. Stator hub, mean and tip sections.

The rotor and stator airfoil geometry were iteratively adjusted to match mass flow and pressure ratio at an adequate stage efficiency. Figure 6 and 7 show the result of the airfoil geometry for rotor and stator at hub, mean and tip sections. At rotor tip the typical wedge-shape profiles are observable.

5.0 NUMERICAL SETUP

For mesh generation the commercial semi-automatic grid generator *NUMECA Autogrid 5* was used. The grid generation process of inlet and outlet duct and rotor and stator domain is controlled by scripts. Inlet and outlet duct have an axial length upstream respectively downstream of the stage of one and a half casing diameter. Figure 8 shows the numerical domain which covers one rotor blade and three stator blades in order to assure equal dimensions in circumferential direction. In a grid sensitivity study, mass flow, pressure ratio and stage efficiency were evaluated and led to 3.4 million nodes for the whole domain. The grid criteria were also examined. To conclude, the minimum skewness angle is below 22° , maximum aspect ratio is below 7000 and maximum expansion ratio is below 2.5.

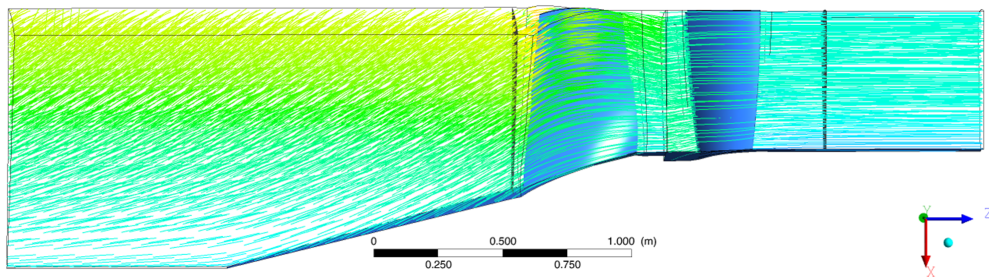


Figure 8. Numerical domain.

The 3D Reynolds-averaged Navier-Stokes (3D-RANS) simulations performed in this paper were done with the commercial solver *ANSYS CFX 17.0*. Hydraulic smooth walls were assumed at each blade, shroud and hub surfaces except of the hub inlet front part which uses free slip walls. The numerical domain was simulated with pitch periodic boundaries. The undistorted inlet flow is supposed to be subsonic with a low turbulence level. Inlet boundary conditions such as total temperature and pressure were taken from the *GasTurb* performance model. At TOC total temperature and pressure yield to 240.4 K and 30666 Pa . The mixing plane between rotor and stator blades averages the velocity. In accordance with [8] the $k - \omega$ turbulence model was used for numerical simulations. The solution at design point was fully converged with RMS residuals below 5×10^{-5} . The maximum dimensionless wall distance y^+ for all walls, rotor and stator blades were around 2 for the design speed line.

6.0 FAN STAGE PERFORMANCE

6.1 Fan stage map

The fan map was generated by varying the outlet pressure for each changed rotational speed. Figure 9 shows PR and stage efficiency depending on reduced mass flow. Furthermore, the operating points listed in Tab. 1 are added to the figure. The normal operating points such as case 1 (top of climb, AEO), 2 (cruise, AEO), 5 (take-off, AEO), 8 (landing, AEO) and 11 (cruise, AEO) are shown in Fig. 9 as black filled symbols. It is important to mention that the aim of the presented fan stage is not to achieve a better design compared to today's fan design but rather having an adequate starting point for future distortion investigations. Moreover, the surge line of the standard map which is used in *GasTurb* is also shown in Fig. 9.

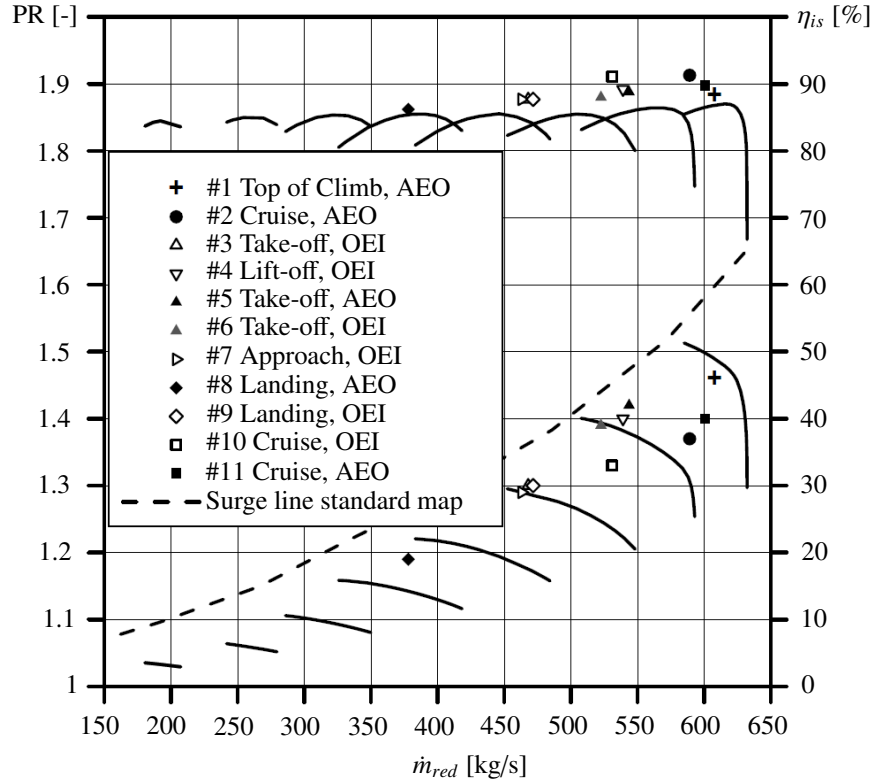


Figure 9. Fan map including all operating points from Tab. 1.

Table 2
Comparing standard map and preliminary UHBR fan stage map implemented into the GasTurb engine model

| Case | Operating Point | ΔSFC [%] | ΔSM [%] | $\Delta SM_{safety, standard}$ [%] | $\Delta SM_{safety, UHBR}$ [%] |
|------|----------------------------|---------------------|--------------------|---------------------------------------|-----------------------------------|
| 1 | Top of Climb, AEO | +4.0 | -10.2 | +30.5 | +20.3 |
| 2 | Cruise, AEO | +6.1 | -7.4 | +39.4 | +32.0 |
| 3 | Take-off, OEI ¹ | +2.7 | -13.2 | +8.8 | -4.3 |
| 4 | Lift-off point, OEI | +1.9 | -5.7 | +4.2 | -1.5 |
| 5 | Take-off, AEO | +2.3 | -5.5 | -0.1 | -5.6 |
| 6 | Take-off, OEI | +1.7 | -25.9 | +0.6 | -4.7 |
| 7 | Approach, OEI ¹ | +2.7 | -14.6 | +10.1 | -4.5 |
| 8 | Landing, AEO ¹ | +3.0 | -25.3 | +22.9 | -2.4 |
| 9 | Landing, OEI | +2.4 | -11.8 | +7.8 | -4.1 |
| 10 | Cruise, OEI | +5.5 | -5.2 | +23.9 | +18.8 |
| 11 | Cruise, AEO | +5.3 | -8.7 | +33.7 | +25.1 |

¹ = EASA CS-25.

As mentioned earlier, the *GasTurb* model was designed by extrapolating trends from Grieb [12] in order to design an UHBR engine with a technology readiness level of 2015. Hence, the efficiency lines clearly shows the lower level compared to the *GasTurb* model which is based on current technology. In average, the operating points from the extrapolated trends are approx. five percent higher compared to the presented preliminary fan stage design. In order to give a statement about the engine *SFC*, the numerical map generated from CFD was implemented into the UHBR engine model. The reason for that is that in general, *GasTurb* uses standardized maps which rely on open literature characteristics [21]. Those maps are scaled based on the design point specification including mass flow, *PR* and efficiency. Hence, in the present study the numerical determined fan map was implemented into the UHBR engine model without any scaling to estimate the engine *SFC* for each operating point separately. Table 2 shows the higher change in *SFC* due to the UHBR fan map. Thereby, the *SFC* change is calculated as

$$\Delta SFC = \frac{SFC_{UHBR \text{ fan map}} - SFC_{standard \text{ GasTurb fan map}}}{SFC_{standard \text{ GasTurb fan map}}}. \quad \dots (7)$$

As expected the *SFC* is increased for the UHBR fan map. This is a result of the preliminary design philosophy compared to current high-fidelity fan stage designs. Taking into account only normal operating points where all engines are operating an average in *SFC* difference of around four percent is observed. This corresponds to the impression one may have regarding the efficiency lines in Fig. 9.

More importantly, the pressure lines indicate that all operating points are below the surge line. This is even more relevant for the normal operating cases (#1, #2, #5, #8 and #11). However, the low surge margin of several cases has to be mentioned as well. The *GasTurb* model was designed by assuring a surge margin at constant mass flow of about 15 percent. Referring to Bräunling [16] this is the recommended distance to the surge line. Table 2 shows the drop in surge margin ΔSM for each operating point comparing standard and UHBR fan map. As expected in all cases a drop in *SM* is experience ranging from -5.2 for cruise to -25.7 percent for take off with AEO. The negative value means a lower surge margin for the UHBR compared to the standard standard fan map.

Setting the recommended 15 percent as a safety margin to the surge line, Tab. 2 also shows the distance to this safety margin for the standard $\Delta M_{safety, standard}$ and the UHBR $\Delta M_{safety, UHBR}$ map. Positive values correspond to a larger distance in the favorable direction away from the 15 percent safety margin distance. Hence, an even larger surge line distance is achieved. The surge margin distance to the safety range for the standard map $\Delta M_{safety, standard}$ confirms the design intent made for the UHBR engine model in *GasTurb*. Except of the very low negative margin for the cases 5 and 6 all other operating points are characterized by a large distance to the 15 percent safety surge margin. Implementing the unscaled numerical UHBR fan map the change to the safety surge margin is clearly visible. The UHBR fan map indicates larger negative values which means that the safety margin of 15 percent to the surge line cannot be maintained. In case of transient maneuver especially the low speed cases will have the largest difficulties to operate safely. The problems will grow even more after a longer operation when the engine is degraded.

Besides the inflow investigations, future research will also focus on varying the bypass nozzle area to estimate the enhancement for fan performance. From the engine performance perspective, Woodward et al. [22] and Hall and Crichton [13] highlighted the benefits emerged with a variable fan nozzle. Additionally, the results of the present study show that future

UHBR fan stages may have surge margin issues and that a variable bypass nozzle for future designs may be one option to operate the engine safely. Having a variable pitch fan rotor may be another option for future designs.

6.2 Fan stage behavior with nacelle inflow

The nacelle flow was delivered by a subproject within the CRC 880. The nacelle is based on the dimensions which rely on the previous described *GasTurb* engine model. The numerical setup of the nacelle consisted of an isolated axisymmetric nacelle without a wing at TOC condition (case 1 in Tab. 1). At fan face total pressure and temperature distribution were extracted and impressed as boundary conditions on the plane directly in front of the fan leading edge which is shown in Fig. 8. Obviously, the duct in front of this plane was cut away and hence, not simulated.

In order to achieve the TOC operating point in Fig. 9 the rotational speed of the fan rotor had to be reduced to 2920 *rpm*. At a reduced mass flow of 607 *kg/sec* and a PR of 1.45 the preliminary fan stage achieved an isentropic efficiency of 87.6 percent which is about one percent higher compared to the numerical setup described in the previous section.

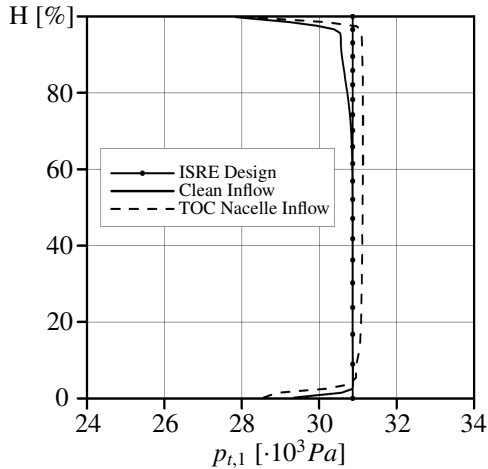


Figure 10. Total pressure distribution at rotor inlet.

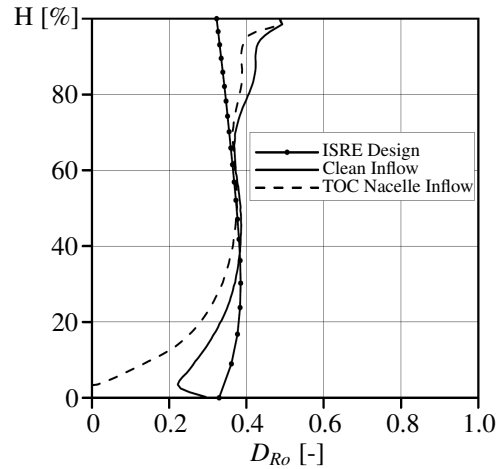


Figure 11. Rotor diffusion factor distribution.

The difference in total pressure distribution can be observed in Fig. 10. In general, the simulations are in accordance with the constant pressure distribution along blade height for the ISRE design intent. Exempt therefrom is the flow near hub and tip due to the boundary layer.

Regarding the numerical setup with inlet duct, at outer radii the blockage as a result of the larger duct in front of the stage and hence, evolved boundary layer is shown. Therefore, the rotor diffusion factor is increased at outer blade radii, cf. Fig. 11. In transonic fan stage design the outer blade sections are more dominant regarding the stage performance due to supersonic inflow and resulting shock structures. As a result of the larger blade loading for the numerical setup with intake duct the blade loss is increased and hence, the efficiency lower.

On the other hand, for the nacelle inflow setup the blade sections at inner radii experience a much larger blockage respectively lower axial velocity seen in Fig. 12. The reduced axial

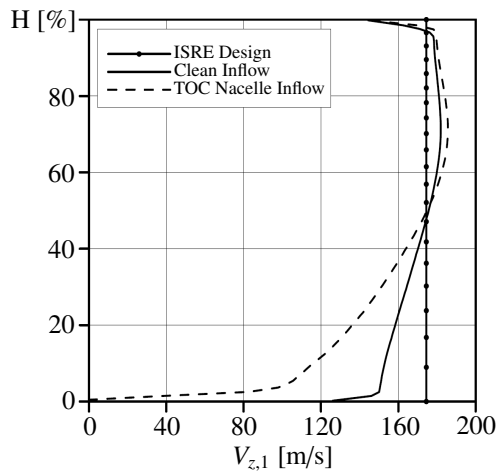


Figure 12. Axial velocity distribution at rotor inlet.

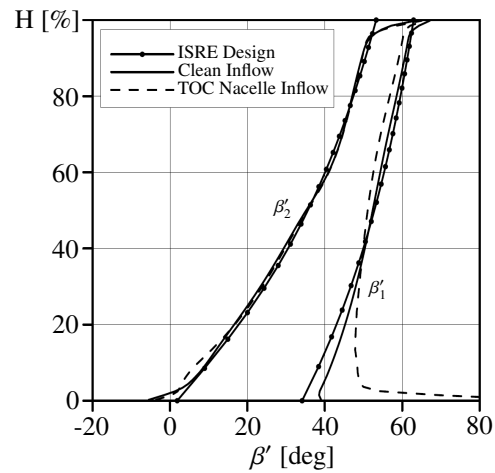


Figure 13. Relative flow angles distributions at rotor.

velocity approaching the rotor leading edge requires larger relative inflow angles (Fig. 13). Changing the rotational speed also modifies the velocity triangles. Even with that modification, the relative inflow angles at inner radii are still larger when comparing the numerical setup with intake duct at TOC inflow condition. However, Fig. 13 illustrates that the rotor sections are able to handle the large inflow angles in a positive manner. This arises from the low blade loading at inner radii too. The rotor sections balance the inflow and hence, the relative flow angle at rotor trailing edge is in accordance to the desired design intent.

7.0 CONCLUSION

In the present study a closed loop design starting with the engine performance model based on aircraft specifications to an assessment of a preliminary fan stage design was shown. For the engine performance model eleven operating points needed to be met. The engine was designed by having an ultra-high bypass ratio of 17 with an overall pressure ratio of 70 to achieve a low specific fuel consumption. Based on the engine model and in particular mass flow, pressure ratio, engine dimensions and also ambient conditions a preliminary fan design tool was developed starting with the conceptualization of the meridional plane for annulus area and radial distribution of flow condition parameters. The preliminary meridional plane design is based on the isentropic simple radial equilibrium equation. Taking into account unique incidence the blading was estimated in an iterative procedure. The developed preliminary fan stage achieved a peak isentropic efficiency of 87.0 percent. Using TOC nacelle flow as inlet boundary condition a one percent larger efficiency was achieved. Implementing the UHBR fan map generated with CFD instead of the standard map in the engine performance model shows a reduction in surge margin of more than 9 percent in average for normal operating points. This results in safety issues when operating UHBR fan stages.

To conclude, the results of the numerical simulations of the preliminary fan stage design are in a good agreement with the design intent. In the on-going research project further inflow distortions regarding the fan stage performance will be investigated. Fan performance benefits with varying bypass nozzle area for UHBR engines has to be studied as well in the future.

ACKNOWLEDGEMENTS

The authors gratefully acknowledge the funding as part of the Coordinated Research Centre 880 (Sonderforschungsbereich 880, SFB 880) provided by the German Research Foundation (Deutsche Forschungsgemeinschaft, DFG).

REFERENCES

- [1] International Air Transport Association (IATA). IATA Forecasts Passenger Demand to Double Over 20 Years. <http://www.iata.org/pressroom/pr/Pages/2016-10-18-02.aspx> (last access: 23/05/2017), October 2016.
- [2] Advisory Council for Aeronautics Research In Europe (ACARE). A Vision for 2020. 2001.
- [3] Advisory Council for Aeronautics Research In Europe (ACARE). Flightpath 2050 - Europe's Vision for Aviation. 2011.
- [4] David L. Daggett, Stephen T. Brown, and Ron T. Kawai. Ultra-efficient engine diameter study. *NASA/CR-2003-212309*, May 2003.
- [5] J.P. Gostelow, K.W. Krabacher, and L.H. Smith Jr. Performance comparisons of high mach number compressor rotor blading. *NASA CR-1256*, 1968.
- [6] W. N. Dalton, D. B. Elliot, and K. L. Nickols. Design of a low speed fan stage for noise suppression. (NASA/CR-1999-208682, Allison-EDR-17923), February 1999.
- [7] Daniel Crichton, Liping Xu, and Cesare A. Hall. Preliminary fan design for a silent aircraft. *Journal of Turbomachinery*, 129(1):184–191, February 2006.
- [8] Burak Kaplan. Design of an advanced fan stage with ultra high bypass ratio and comparison with experimental results. Technical report, DLR-Forschungsbericht. DLR-FB-2010-20, April 2010.
- [9] W. Heinze and T. Weiss. Main Data Sheet - A/C Type: SFB880 Reference Aircraft REF3-2015. Technical report, Institute of Aircraft Design and Lightweight Structures, TU Braunschweig, June 2015.
- [10] W. Heinze, C.M. Oesterheld, and P. Horst. Multidisziplinäres Flugzeugentwurfsverfahren PrADO - Programmwurf und Anwendung im Rahmen von Flugzeug-Konzeptstudien. *Jahrbuch der DGLR-Jahrestagung 2001 in Hamburg*, 2001.
- [11] Joachim Kurzke. *GasTurb 12 - Design and Off-Design Performance of Gas Turbines*.
- [12] Hubert Grieb. *Verdichter fuer Turbo-Flugtriebwerke*. Springer-Verlag, Berlin, 2009.
- [13] Cesare A. Hall and Daniel Crichton. Engine design studies for a silent aircraft. *Journal of Turbomachinery*, 129(3):479–487, July 2006.
- [14] Members of Staff of Lewis Research Center. *Aerodynamic Design of Axial-Flow Compressors - NASA SP-36*. National Aeronautics and Space Administration (NASA), 1965.
- [15] N.A. Cumpsty. *Compressor Aerodynamics*. Krieger Publishing Company, 2004.
- [16] Willy J. G. Braeunling. *Flugzeugtriebwerke - Grundlagen, Aero-Thermodynamik, ideale und reale Kreisprozesse, Thermische Turbomaschinen, Komponenten, Emissionen und Systeme*. Springer-Verlag, 3. edition, Berlin, 2009.

-
- [17] Hermann Schlichting and Erich Truckenbrodt. *Aerodynamik des Flugzeuges (Band 1) - Grundlagen aus der Stroemungsmechanik, Aerodynamik des Tragfluegels (Teil 1)*. Springer-Verlag, Berlin, Deutschland, 2. edition, 1967.
 - [18] A. J. Wennerstrom. *Design of Highly Loaded Axial-Flow Fans and Compressors*. Concepts ETI, 2001.
 - [19] Ira H. Abbott and Albert E. von Doenhoff. *Theory of Wing Sections: Including a Summary of Airfoil Data*. Dover Books on Aeronautical Engineering. Dover Publications, 1959.
 - [20] H.I.H. Saravanamuttoo, G.F.C. Rogers, H. Cohen, and P.V. Straznicky. *Gas Turbine Theory*. Pearson Education Limited, 6. edition edition, Essex, England, 2009.
 - [21] Joachim Kurzke. *Smooth C 8.2 - Preparing Compressor Maps for Gas Turbine Performance Modeling*, 2008.
 - [22] Richard P. Woodward, Christopher E. Hughes, and Gary G. Podboy. Fan noise reduction with increased bypass nozzle area. *Journal of Aircraft*, 43(6):1719–1725, November 2006.